Title
The role of mitochondrially derived ATP in synaptic vesicle recycling.

Journal
Journal of Biological Chemistry, 290(37)

Authors
Pathak, Divya
Shields, Lauren
Mendelsohn, Bryce
et al.

Publication Date
2015-09-11

DOI
10.1074/jbc.M115.656405

Peer reviewed

THE JOURNAL OF BIOLOGICAL CHEMISTRY VOL. 290, NO. 37, pp. 22325–22336, September 11, 2015

The Role of Mitochondrially Derived ATP in Synaptic Vesicle Recycling*◆

Received for publication, April 7, 2015, and in revised form, June 19, 2015 Published, JBC Papers in Press, June 30, 2015, DOI 10.1074/jbc.M115.656405

Divya Pathak[‡1], Lauren Y. Shields[‡§1,2], Bryce A. Mendelsohn[‡¶3], Dominik Haddad[‡1], Wei Lin[‡1], Akos A. Gerencser[‖], Hwajin Kim[‡1], Martin D. Brand[‖], Robert H. Edwards[§], and Ken Nakamura[‡§1,4]

From the [‡]Gladstone Institute of Neurological Disease, San Francisco, California 94158, the [§]Department of Neurology and Graduate Programs in Neuroscience and Biomedical Sciences, University of California at San Francisco, San Francisco, California 94158, the [¶]Department of Pediatrics, University of California at San Francisco, San Francisco, California 94143, and the [‖]Buck Institute for Research on Aging, Novato, California 94945

Background: The ATP requirements of synaptic vesicle release are poorly understood.
Results: Mitochondrially derived ATP supports the function of boutons with and without mitochondria. Respiratory dysfunction selectively blocks the reinternalization of synaptic vesicles.
Conclusion: ATP diffuses rapidly in axons to support synaptic vesicle recycling. Mitochondrial dysfunction decreases synaptic energy and impairs function.
Significance: Understanding energy requirements will help determine how energy failure contributes to neurodegeneration.

Synaptic mitochondria are thought to be critical in supporting neuronal energy requirements at the synapse, and bioenergetic failure at the synapse may impair neural transmission and contribute to neurodegeneration. However, little is known about the energy requirements of synaptic vesicle release or whether these energy requirements go unmet in disease, primarily due to a lack of appropriate tools and sensitive assays. To determine the dependence of synaptic vesicle cycling on mitochondrially derived ATP levels, we developed two complementary assays sensitive to mitochondrially derived ATP in individual, living hippocampal boutons. The first is a functional assay for mitochondrially derived ATP that uses the extent of synaptic vesicle cycling as a surrogate for ATP level. The second uses ATP FRET sensors to directly measure ATP at the synapse. Using these assays, we show that endocytosis has high ATP requirements and that vesicle reacidification and exocytosis require comparatively little energy. We then show that to meet these energy needs, mitochondrially derived ATP is rapidly dispersed in axons, thereby maintaining near normal levels of ATP even in boutons lacking mitochondria. As a result, the capacity for synaptic vesicle cycling is similar in boutons without mitochondria as in those with mitochondria. Finally, we show that loss of a key respiratory subunit implicated in Leigh disease markedly decreases mitochondrially derived ATP levels in axons, thus inhibiting synaptic vesicle cycling. This proves that mitochondria-based energy failure can occur and be detected in individual neurons that have a genetic mitochondrial defect.

Mitochondria likely provide the main source of ATP that supports synaptic transmission, whereas anaerobic respiration from glycolysis contributes much less ATP (1). Yet, surprisingly, less than half of all synaptic boutons in adult rodent hippocampus or in cultured hippocampal neurons contain mitochondria (2, 3). This raises questions about where synaptic ATP originates, how it is distributed among boutons, and how much energy is needed to support synaptic transmission. Dysfunction of axonal mitochondria may also have a critical role in the pathogenesis of neurodegenerative diseases, including Parkinson disease and Alzheimers disease. Indeed, multiple neurodegenerative pathways are thought to converge on energy failure, and synaptic terminals degenerate early in many neurodegenerative diseases associated with impaired energy metabolism (4–6). These findings indicate that significant changes in bioenergetic function may occur that are restricted to or occur first in the neuronal processes. In addition, axonal mitochondria have unique properties and exist in distinct microenvironments; thus, it is critical that we first understand the bioenergetics of intact axons. But surprisingly, energy failure has never been proved to occur in dysfunctional or dying disease-affected neurons or in the intact neurons used in genetic disease models (6). Therefore, without knowing the normal energy requirements of neurons or how much energy depletion occurs in disease, we cannot know whether energy failure plays a causative role in degeneration.

Our understanding of neuronal bioenergetics has been limited because the established assays have insufficient resolution (6). Although respiration, glycolysis, and ATP can be measured in whole neuronal cultures, these approaches cannot accurately factor out ATP contributions from glia or provide subcellular spatial resolution. Synaptosome analyses continue to elucidate synaptic bioenergetic functions, but they are challenging in spe-

* This work was supported, in whole or in part, by National Institutes of Health Grant RR018928 (to the Gladstone Institutes). This work was also supported by Betty Brown's Family and the Joan and David Traitel Family Trust. The authors declare that they have no conflicts of interest with the contents of this article.
◆ This article was selected as a Paper of the Week.
[1] Supported by a Burroughs-Wellcome Medical Scientist Fund Career Award and National Institutes of Health Grants 1KO8NS062954-01A1, 1RO1NS091902-01, and P30NS069496 from the NINDS.
[2] Supported by a National Science Foundation graduate research fellowship.
[3] Supported by the Pediatric Scientist Development Program.
[4] To whom correspondence should be addressed: Gladstone Institute of Neurological Disease, San Francisco, CA 94158. Tel.: 415-734-2550; Fax: 415-355-0824; E-mail: ken.nakamura@gladstone.ucsf.edu.

cific neuronal types (7) and are also subject to artifacts related to the isolation process. Mitochondrial membrane potential can be studied in intact neurons (8), but this is difficult in small axonal mitochondria and provides only indirect bioenergetic information. In addition, the mass and distribution of axonal mitochondria are just as important as their function (6).

To measure mitochondrially derived energy at the synapse, we designed sensitive ATP assays that suppress glycolysis so neurons must rely on mitochondria for energy. Using these assays, we identified the energy threshold needed to support synaptic vesicle cycling and showed that, when ATP drops below this threshold, endocytosis is blocked at or before the vesicle scission step. We showed that, to meet these energy needs, ATP rapidly disperses in axons, resulting in near normal ATP levels even in boutons lacking mitochondria. Finally, we showed that loss of a mitochondrial protein known to cause neurodegeneration (Leigh disease) also causes mitochondrially derived energy levels to drop enough in individual neurons to impair synaptic function, thus proving that mitochondrion-based energy failure can occur and be detected in individual neurons with genetic mitochondrial defects.

Experimental Procedures

Molecular Biology—All constructs were subcloned or cloned into the pCAGGS vector downstream of the chicken actin promoter (9). $AT1.03^{YEMK}$ and $AT^{R122K/R126K}$ fluorescence resonance energy transfer (FRET) sensors (which use a variant of CFP[5] (mseCFP) as the donor fluorophore and YFP (circularly permuted monomeric Venus) as the acceptor fluorophore, surrounding an ATP-binding protein) were the kind gifts from Hiromi Imamura (Kyoto University) and Hiroyuki Noji (Osaka University) (10). VGLUT1-pHluorin, mCherry-synaptophysin, mitoGFP, and the direct CFP-YFP fusion have been described (9, 11–13). Mito-FarRed (TagRFP657 fused to the mitochondrial targeting sequence, cytochrome *c* oxidase subunit VIII) and mTagBFP (used to make mito-mTagBFP) were kind gifts from Vladislav Verkhusha (Albert Einstein College of Medicine) (14, 15), and Cre recombinase (Cre) was from Addgene.

Cell Culture—Postnatal hippocampal neurons used in live-imaging experiments were prepared from P0 rat or mouse pups as described (16–18) and were plated in medium containing 5% fetal bovine serum at a density of 650 cells/mm^2. 10 μM 5-fluoro-2-deoxyuridine and 10 μM uridine were added on day 4 *in vitro* to prevent glial overgrowth. Floxed *Ndufs4* mice (19) used to prepare mouse hippocampal neurons were obtained from Richard Palmiter (University of Washington, Seattle). For sparsely transfected neuronal cultures, 325 untransfected neurons/mm^2 and 32 transfected neurons/mm^2 were plated. Cells for imaging were transiently transfected by electroporation (Amaxa). Hippocampal neurons for Seahorse experiments were prepared from embryonic day (E)18 embryos (21), plated in serum-free medium at a density of 5×10^4 cells per well in a 96-well polystyrene microplate, and cultured for 11 days before analysis. Rat glial cultures were prepared from P0 rats and plated 3 days earlier at 6×10^4 cells per well on the same 96-well microplate (16).

Respiration and Glycolysis—The extracellular acidification rate (ECAR, a surrogate for glycolysis) and oxygen consumption rate (OCR, to assess mitochondrial respiration) were measured using a Seahorse XF96 Extracellular Flux Analyzer (Seahorse Bioscience). Cells were washed and preincubated for 30 min in Seahorse assay medium (pH 7.4) containing substrates of interest (30 mM glucose, 10 mM pyruvate, or both). OCR and ECAR were measured at baseline and again after sequential addition of respiratory inhibitors at final concentrations of 1 μM carbonyl cyanide-4-(trifluoromethoxy)phenylhydrazone, a protonophore that uncouples oxidative phosphorylation in mitochondria, 2 μM rotenone (an inhibitor of mitochondrial complex I), or 4 μM oligomycin (inhibitor of ATP synthase). After each run, cells were fixed with 4% paraformaldehyde and stained with microtubule-associated protein 2 (MAP2) and glial fibrillary acidic protein (GFAP) to distinguish glia from neurons. To correct for the glial contribution, we estimated the glial content in each well by creating a ratiometric image of GFAP staining/MAP2 staining, which allowed us to clearly resolve glia from neurons (this was done because both antibodies had some nonspecific staining). In parallel, we used pure astrocyte cultures to estimate the contribution of an equivalent number of astrocytes. Neuronal respiration corrected for glial contamination was calculated based on the following formula: neuron OCR = neuronal culture OCR − (glia OCR, the respiration of pure glia cultures)·(glial content neuronal culture/glial content of pure glial culture).

Single Synaptosome Imaging—Single synaptosome imaging was performed using reported methods (22). Briefly, cortical synaptosomes (1 μg of protein/well) from adult FVB mice were attached to polyethyleneimine (1:15,000 w/v %) plus geltrex (1 v/v %)-coated cover glass-bottomed microplates (Whatman) by centrifugation and were incubated with 65 nM MitoTracker Green and 2.5 μM fura-4F AM in pH 7.4 buffer containing 3.5 mM KCl, 120 mM NaCl, 0.4 mM KH_2PO_4, 1.2 mM Na_2SO_4, 15 mM D-glucose, 10 mM pyruvate, and 10 mM TES for 30 min at 37 °C. Buffer was then replaced with fresh buffer containing 1.3 mM $CaCl_2$, 0.4% (w/v) fatty acid-free bovine serum albumin, and 5 nM tetramethylrhodamine methyl ester (TMRM), and wide-field images were acquired with a Nikon Eclipse Ti-PFS inverted epifluorescence microscope and an S-Fluor 40 × 1.4 NA oil lens with the filters (excitation, dichroic mirror, and emission in nm/bandwidth) for TMRM (543/22, 562, 617/73; 150-ms exposure time), MitoTracker Green (472/30, 505, 520/35; 150 ms) and fura-4F (340/26 (250 ms) and 387/11 (125 ms), 409, 510/84). Four time points were acquired at 5-min intervals, and the buffer was replaced with fresh buffer containing the desired substrate composition after the second time point. Fields of ~30,000 synaptosomes were imaged using 4 × 4 tiling in each time point. Because fura-4F became essentially saturated in synaptosomes with dysregulated Ca^{2+} homeostasis, the fraction of individual synaptosomes with a higher fura-4F excitation ratio than a fixed threshold (ratio of 2, equivalent to ~6 μM) was determined. This was performed using automated

[5] The abbreviations used are: CFP, cyan fluorescent protein; 2DG, 2-deoxyglucose; ECAR, extracellular acidification rate; GFAP, glial fibrillary acidic protein; IAA, iodoacetate, OCR, oxygen consumption rate; E, embryonic day; TES, 2-{[2-hydroxy-1,1-bis(hydroxymethyl)ethyl]amino}ethanesulfonic acid; TMRM, tetramethylrhodamine methyl ester.

image segmentation in Image Analyst MKII (Image Analyst Software, Novato, CA).

ATP Calibration Assays—HeLa cells and neurons were permeabilized by incubation with XF-PMP reagent (1 nM for HeLa, 1.25 nM for neurons; Seahorse Bioscience) for 4 min in a cytosolic buffer (140 mM KCl, 6 mM NaCl, 1 mM $MgCl_2$, 0.465 mM $CaCl_2$, 2 mM EGTA, and 12.5 mM HEPES, all at pH 7.0) (23) at room temperature and then washed and incubated for an additional 26 min. Buffer was then replaced with fresh buffer containing increasing concentrations of ATP, and the FRET was measured.

Live Imaging—Neurons were cultured for 11 days (rat neurons) or 8–9 days (mouse neurons) and then imaged live in Tyrode's medium (pH 7.4; in mM: 127 NaCl, 10 HEPES-NaOH, 2.5 KCl, 2 $MgCl_2$, and 2 $CaCl_2$, with either 30 mM glucose and/or 10 mM pyruvate, unless otherwise specified) using a Nikon CFI Plan Apo ×40/0.95 air objective on a Nikon Ti-E inverted microscope with an iXon EMCCD camera (Andor Technology), and a perfusion valve control system (VC-8, Warner Instruments), controlled by Metamorph software (Molecular Devices). All buffer changes and drug additions were made by perfusion except for MES (Fig. 6*C*), which was directly injected into the imaging chamber to achieve immediate mixing. Field stimulations were done using an A385 current isolator and a SYS-A310 Accu pulser signal generator (World Precision Instruments).

VGLUT1-pHluorin fluorescence images were obtained (490/20 excitation, 535/50 emission, Chroma), and regions of interest were drawn over synaptic boutons using Metamorph software. Synaptic boutons were identified based on co-localization with mCherry-synaptophysin and an increase in pHluorin fluorescence after we applied ammonium chloride (50 mM). For each bouton, the background-subtracted change in fluorescence at each time point was normalized to the fluorescence in ammonium chloride (which estimates the total synaptic vesicle pool size) (16), measured at the end of each run. The baseline fluorescence intensity was set to zero either 5 or 20 s before the first stimulation and then again before the second stimulation after any change in substrate or drug addition.

For FRET experiments, sequential images were taken in the CFP (430/24 excitation, 470/24 emission), YFP (500/20 excitation, 535/30 emission), and FRET channels (430/24 excitation, 535/30 emission) using an ET enhanced CFP/enhanced YFP filter set (Chroma). Synaptic boutons were again identified based on co-localization with mCherry-synaptophysin or for experiments with mito-FarRED by morphology. Synaptic boutons were classified as containing or lacking stationary mitochondria (identified based on co-expression of either mito-mTagBFP or mito-FarRed) based on the respective presence or absence of a mitochondrion within the bouton in images taken immediately before and after the imaging run. Those boutons that contained mitochondria only at the beginning or end of the imaging period were excluded from analysis.

The FRET/donor ratio was calculated for each bouton as described (24), where $FRET = (I_{FRET} - I_{CFP}\cdot BT_{CFP} - I_{YFP}\cdot BT_{YFP})/I_{CFP}$, where I_X is the background-corrected fluorescence intensity measured in a given channel. BT_{CFP} (donor bleed through) and BT_{YFP} (direct excitation of the acceptor) were calculated by expressing CFP and YFP individually and then determining the ratios of I_{FRET}/I_{CFP} and I_{FRET}/I_{YFP}, respectively.

Immunocytochemistry—Cells were fixed for 15 min in phosphate-buffered saline (PBS) containing 4% paraformaldehyde and immunostained in PBS containing 5% fetal bovine serum and 0.2% Triton X-100. Total neurons were detected using an antibody to MAP2 (Millipore, catalogue no. MAB3418), astrocytes with GFAP (rabbit clone, Sigma, catalogue no. G9269), mitochondria with Tom20 (rabbit, Santa Cruz Biotechnology, catalogue no. SC-11415), and mCherry with DsRED (rabbit, Clontech, catalogue no. 632496).

Results

Substrate Availability Determines Extent of Reliance on Mitochondria for ATP—Physiologic brain glucose levels (≈1–1.5 mM (25, 26)) are far lower than those typically used to culture neurons and perform mitochondrial function assays (≈25–30 mM). Under these high glucose conditions, glycolysis likely compensates for any respiratory deficits and obscures our ability to detect whether and how any respiratory deficits affect neuronal function/survival. Therefore, to develop sensitive assays to measure mitochondrially derived ATP in neurons, we first delineated how the relative ATP contributions of aerobic and anaerobic respiration are influenced by substrate availability. Using a Seahorse instrument, we measured the rates of respiration and glycolysis in E18 hippocampal cultures grown for 11 days. In 30 mM glucose (a supra-physiological concentration often used in cell culture and imaging buffers) basal and maximal OCRs were low, indicating little aerobic respiration (Fig. 1). But when pyruvate (10 mM) was substituted for glucose for 30 min, respiration increased, as did the ratio of OCR to ECAR (Fig. 1*D*), indicating a greater reliance on aerobic respiration. Importantly, these data reflect bioenergetic changes in neurons specifically, as we both minimized glial content (using embryonic cultures grown in serum-free medium) and used parallel glia-only cultures to correct for the ATP contribution of the remaining glia. As such, our normalized glial OCR calculations show that glia only minimally contribute to the total OCR regardless of substrate (Fig. 1). Therefore, neurons derive more energy from mitochondrial respiration when exposed to pyruvate, but they rely more on glycolysis when exposed only to high glucose levels. So, we hypothesized that to detect the consequences of lower mitochondrial ATP levels, we should use substrates that promote aerobic respiration and minimize glycolysis.

To test this at the synapse, which is the first area to degenerate in several neurodegenerative diseases involving mitochondria (4, 5), we first examined how the substrate affects the ATP-dependent capacity of synaptosomes to maintain low calcium levels (7). We used fluorescence microscopy of the low affinity Ca^{2+} probe fura-4F AM to measure the loss of Ca^{2+} homeostasis in single synaptosomes. Most synaptosomes maintained low resting calcium levels (below the sensitive range of fura-4F; <100 nM [Ca^{2+}]) even without substrates in the medium, suggesting that endogenous substrates suffice (Fig. 1*E*). Glycolysis alone also maintained calcium homeostasis, but inhibiting all glycolysis (by iodoacetate; 250 μM), oxidative phosphorylation

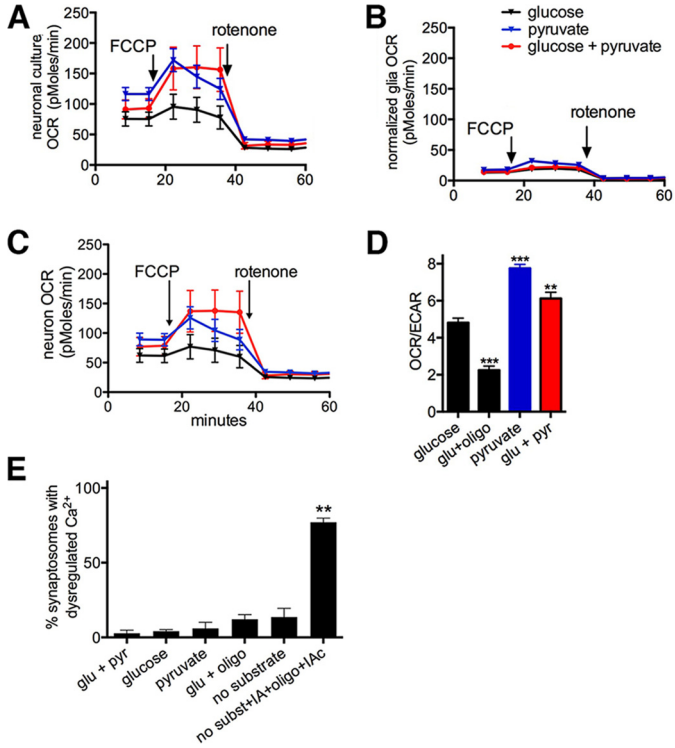

FIGURE 1. **Pyruvate and glucose availability regulates the level of neuronal aerobic and anaerobic energy metabolism.** Aerobic respiration rates (OCR) were measured in 11-day-old primary E18 rat hippocampal neuronal and parallel glia-only cultures with a 96-well Seahorse extracellular flux analyzer. *A,* in neuronal cultures, basal OCR is greater in medium containing 10 mM pyruvate ($p < 0.001$ *versus* 30 mM glucose alone by two-way ANOVA with repeated measures). After carbonyl cyanide-4-(trifluoromethoxy)phenylhydrazone (*FCCP*) addition at the *arrow* (a mitochondrial uncoupler, 1 μM), maximal respiration is greater in medium containing pyruvate ($p < 0.001$) or pyruvate + glucose ($p < 0.01$). Subsequent addition of the mitochondrial complex I inhibitor rotenone (2 μM) blocks respiration and decreases OCR to the same level in all groups. *B,* in comparison, normalized glial respiration rates in parallel glia-only cultures were far lower than neuronal rates. *C,* subtraction of estimated glial contribution to total OCR in neuronal cultures revealed the "neuron OCR," which showed similar results to the total OCR of the neuronal culture. Therefore, although glia constitute a significant proportion of cells even in "pure" neuronal cultures, they respire at much lower levels than neurons, and hence, the overall pattern of neuron-corrected OCR is similar to the total-well OCR. Data are mean ± S.E. from a representative experiment with 5–12 wells/group. *D,* ratio of OCR/ECAR represents the neurons' reliance on aerobic respiration *versus* glycolysis for ATP. When pyruvate is present, neurons rely more on aerobic respiration, but this decreased when we added the ATP synthase inhibitor oligomycin (*oligo*; 4 μM). Data are mean ± S.E. from a representative experiment with 5–12 wells/group. **, $p < 0.01$; ***, $p < 0.001$, *versus* the glucose-only group by one-way ANOVA and Dunnett's post hoc test. *E,* percentage of synaptosomes that failed to maintain Ca^{2+} homeostasis (fura-4F ratio was above 2, equivalent to 6 μM) 15 min after changing to medium containing glucose (*glu*; 15 mM), pyruvate (*pyr*; 10 mM), or neither. Combined inhibition of glycolysis (by iodoacetate, *IAA*; 250 μM), oxidative phosphorylation (by oligomycin; 1 μg/ml), and creatine kinase (by iodoacetamide, *IAc*; 250 μM) caused Ca^{2+} dysregulation in most synaptosomes. Therefore, glycolysis must be suppressed to detect how deficits in mitochondrial ATP production affect Ca^{2+} levels. $n = 4$, data are mean ± S.E. **, $p < 0.01$, by *t* test *versus* glucose + pyruvate.

(oligomycin; 1 μg/ml), and creatine kinase (iodoacetamide; 250 μM) disrupted synaptosome calcium regulation, manifesting in a precipitous increase in [Ca^{2+}] (>6 μM). This suggests that ATP fell below the threshold required to maintain normal low calcium levels. So, because calcium regulation can be supported by either glycolysis or respiration, we must suppress glycolysis to determine how impaired mitochondrial ATP production affects calcium levels.

Aerobic and Glycolytic ATP Requirements of the Synaptic Vesicle Cycle—Synaptic vesicle release may be impaired early in diseases that deplete energy (27), but the ATP requirements of the synaptic vesicle cycle are poorly understood. To investigate how much mitochondrially derived ATP is needed for different phases of the synaptic vesicle cycle, we assessed synaptic vesicle release when neurons were exposed to different substrates. For this and all subsequent live imaging experiments, we studied postnatal hippocampal neurons grown in serum-containing media (16–18). These cultures also include glia, and thus better incorporate glia-neuron interactions that likely influence energy metabolism in neurons (28). To monitor the synaptic vesicle cycle in individual boutons, we used the VGLUT1-pHluorin reporter, which targets a pH-sensitive GFP (pHluorin) to the lumen of synaptic vesicles. pHluorin does not fluoresce in an acidified vesicle, but it does fluoresce when a vesicle fuses and its contents are exposed to the alkaline extracellular environment (9). pHluorin fluorescence is then quenched after endocytosis of the vesicle and subsequent reacidification (Fig. 2).

Postnatal hippocampal neurons were incubated either in buffer containing 30 mM glucose to facilitate aerobic respiration and glycolysis or in buffer lacking glucose but containing 10 mM pyruvate to favor reliance on mitochondria. To determine whether the synaptic vesicle cycle could function in the different buffers for a range of activity levels, we exposed neurons to two commonly used electrical field-stimulation paradigms as follows: a longer but lower frequency stimulation (60 s at 10 Hz) that facilitates the preferential release of vesicles in the recycling pool (total pool of vesicles that can undergo activity-dependent synaptic vesicle cycling (Fig. 2, *A–C*) (29)), or a shorter but higher frequency stimulation (3 s at 30 Hz) that promotes the release of vesicles in the readily releasable pool (vesicles docked and "primed" at the active zone for immediate fusion upon stimulation (Fig. 2, *D* and *E*) (16, 30, 31)).

Synaptic vesicle cycling remained intact with either substrate (glucose or pyruvate) with either stimulation paradigm. But without glucose, the rate that the pHluorin signal returned to baseline was slightly impaired with repetitive 60 s at 10 Hz stimulation (Fig. 2*A*), indicating a small drop-off in endocytosis when glucose was absent. Therefore, because respiration could not fully compensate in this paradigm, some amount of glycolysis was required. These experiments were performed in the presence of glutamate receptor antagonists, 10 μM 6-cyano-7-nitroquinoxaline-2,3-dione and 50 μM DL-2-amino-5-phosphonovaleric acid, to eliminate endogenous network activity, but these antagonists had no detectable impact on our assays (data not shown) and were excluded from subsequent experiments.

Neurons do not store glucose in the form of glycogen (32) and cannot replenish their own glucose supply, so synaptic vesicle cycling that occurs in the absence of glucose but with pyruvate is likely supported by mitochondrially derived ATP. To test this, we applied rotenone (500 nM), which inhibits mitochondrial complex I. With rotenone, endocytosis was completely blocked for cells in pyruvate but not for cells in glucose (Fig. 2, *B* and *E*). Similarly, the ATP synthase inhibitor oligomycin (2.5 μg/ml) also blocked endocytosis, but only in the absence of glucose (Fig. 2*C*). This confirms that endocytosis depends on

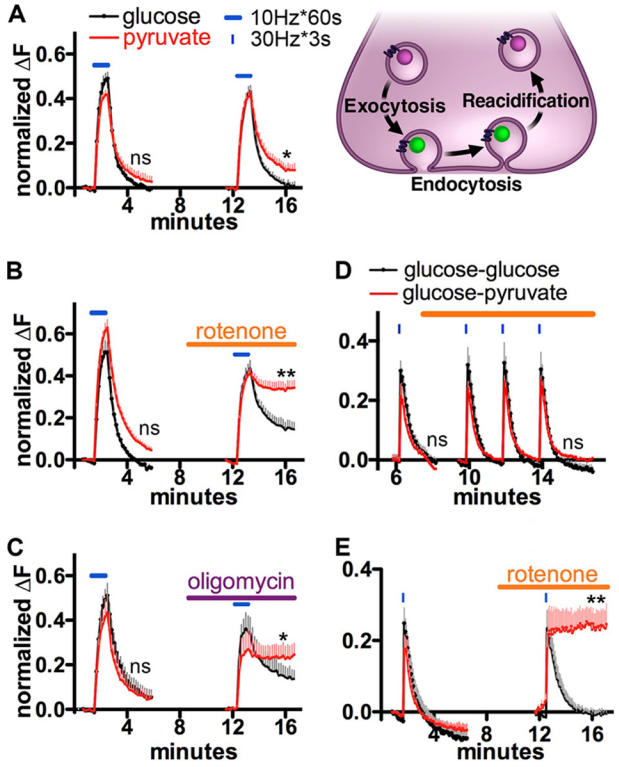

FIGURE 2. **Functional assay for mitochondrially derived ATP reveals differential ATP requirements of the synaptic vesicle cycle.** Synaptic transmission at individual boutons was assessed in hippocampal neurons expressing a pH-sensitive GFP targeted to synaptic vesicles (VGLUT1-pHluorin (9), *diagram top right*). The rise in the curve during electrical stimulation reflects primarily exocytosis, although the downstroke reflects endocytosis and synaptic vesicle reacidification. *A–C,* electrical field stimulation of the recycling pool (*10Hz*60s, horizontal blue lines*). Each *curve* shows the mean change in pHluorin fluorescence (Δ*F*) normalized to the size of the total pool of VGLUT-pHluorin in each bouton (determined by measuring the fluorescence after application of 50 mM NH_4Cl after each run (16, 63)). *A,* without glucose, synaptic vesicle cycling was maintained with pyruvate (*red line*), but repeat stimulation slightly compromised the extent of endocytosis. *B* and *C,* endocytosis without glucose (*red line*) *versus* with glucose (*black line*) depended on mitochondrially derived ATP and was completely blocked by either rotenone (500 nM) or oligomycin (2.5 μg/ml). *D,* electrical stimulation (*30Hz*3s, narrow vertical blue lines*) to release the readily releasable pool. Even without glucose (*orange line*), synaptic vesicle cycling was maintained with pyruvate (glucose-pyruvate, *red line*). *E,* without glucose (*red line*) endocytosis depended on mitochondrially derived ATP and was completely blocked by rotenone. This change in endocytosis provides a functional measure of mitochondrially derived energy. $n = 4–6$ coverslips (110–151 boutons)/group. Data show mean ± S.E. *, $p < 0.05$; **, $p < 0.01$; *ns* = not significant, for extent of endocytosis ((amplitude endocytosis)/(amplitude exocytosis)) with *versus* without glucose by two-way ANOVA with repeated measures and Bonferroni post hoc test.

mitochondrially derived ATP when glycolysis is impaired. In contrast, the rate of exocytosis was largely preserved throughout these trials. In particular, exocytosis was fully preserved with 30Hz*3s stimulation targeting the readily releasable pool (Fig. 2*E*), indicating that little energy is required to release vesicles, especially once primed.

Measuring ATP at the Nerve Terminal—To directly assess the ATP requirements of the synaptic vesicle cycle, we developed an approach to measure ATP in individual synapses. To do this, we obtained ATP FRET sensors (ATeams) (10) that are specifically sensitive to ATP (with no response to ADP, other nucleotide triphosphates, NADH, or dATP) (33, 34) and are resistant to physiologic changes in pH. In HeLa cells, expression of $AT1.03^{YEMK}$ (K_d = 1.2 mM) gave a robust FRET signal that rapidly decreased when aerobic respiration and glycolysis were inhibited with potassium cyanide (KCN, 1 mM) and 2-deoxyglucose (2DG, 10 mM), respectively (Fig. 3*A*). These interventions did not affect the FRET produced by the $AT^{R122K/R126K}$ dead mutant (does not bind ATP) or the direct fusion of CFP and YFP, indicating that the sensor specifically measures ATP.

To calibrate the sensitivity of $AT1.03^{YEMK}$ to ATP levels in living cells, we did an in-cell calibration. We incubated permeabilized HeLa cells with increasing concentrations of exogenous ATP; the FRET progressively increased between 250 μM and 5 mM ATP (Fig. 3, *B* and *C*), which are physiologically relevant ATP concentrations. Because the FRET values plateaued >2 mM, they are most sensitive to ATP changes below ≈2 mM. At baseline, $AT1.03^{YEMK}$ is near the top of its dynamic range in HeLa cells but is not fully saturated, as ATP levels drop instantaneously when we add respiratory/glycolytic inhibitors (Fig. 3*A*).

Based on their similar basal ATP FRET levels and similar FRET of the $AT^{R122K/R126K}$ dead mutant (Fig. 3*D*), HeLa cells and synaptic boutons appear to have similar basal ATP levels (we estimate ≈2–4 mM ATP). Although slightly higher, this is similar to the estimated ATP range recently reported by Rangaraju *et al.* (35) (1.4 mM, 10th to 90th percentiles: ≈0.6–2.6 mM), who used a luciferase-based approach. Our additional permeabilization experiments in single synaptic boutons further confirmed that our probes are sensitive to physiologic ATP levels. A precise calibration was not possible though because the required cytosolic buffers and the permeabilization process made many of the synaptic boutons swell, disappear, or merge with adjacent boutons (Fig. 3*E*). However, these studies confirm that $AT1.03^{YEMK}$ (now simply called the ATP FRET sensor) is sensitive to physiologically relevant changes in ATP levels at the synapse and hence is an appropriate tool to study dynamic changes in ATP at the nerve terminal.

We next used the FRET sensor to monitor ATP in neurons given different substrates. At baseline, basal FRET values were stable in boutons over 25 min of imaging even when both glucose and pyruvate were absent (Fig. 4, *A* and *B*); neurons thus had enough substrates to maintain their basal ATP. But when glycolysis was fully blocked, ATP levels quickly dropped, and this was prevented by adding 10 mM pyruvate (a standard dose that enters cells and then mitochondria via monocarboxylate transporters (MCTs) (36)) to fuel respiration, indicating that respiration is required to support basal ATP when glycolysis is absent (Fig. 4*C*).

Threshold ATP Requirement for Endocytosis—Having developed an approach to monitor ATP levels in synaptic vesicles, we next examined how synaptic vesicle cycling affects presynaptic ATP levels, hypothesizing that neural activity, which increases energy demands, would decrease ATP levels. Indeed, in the presence of glucose and pyruvate, electrical stimulation (10Hz*60s) led to a small but rapid drop in ATP FRET levels that fully recovered within ≈5 min (Fig. 5*A*). Stimulation in pyruvate alone produced a similar decrease in ATP with near complete recovery (Fig. 5*B*), but the lack of complete recovery suggests that some glycolysis is needed (as in Fig. 2*A*). A brief 30Hz*3s stimulation did not affect ATP levels when glucose and

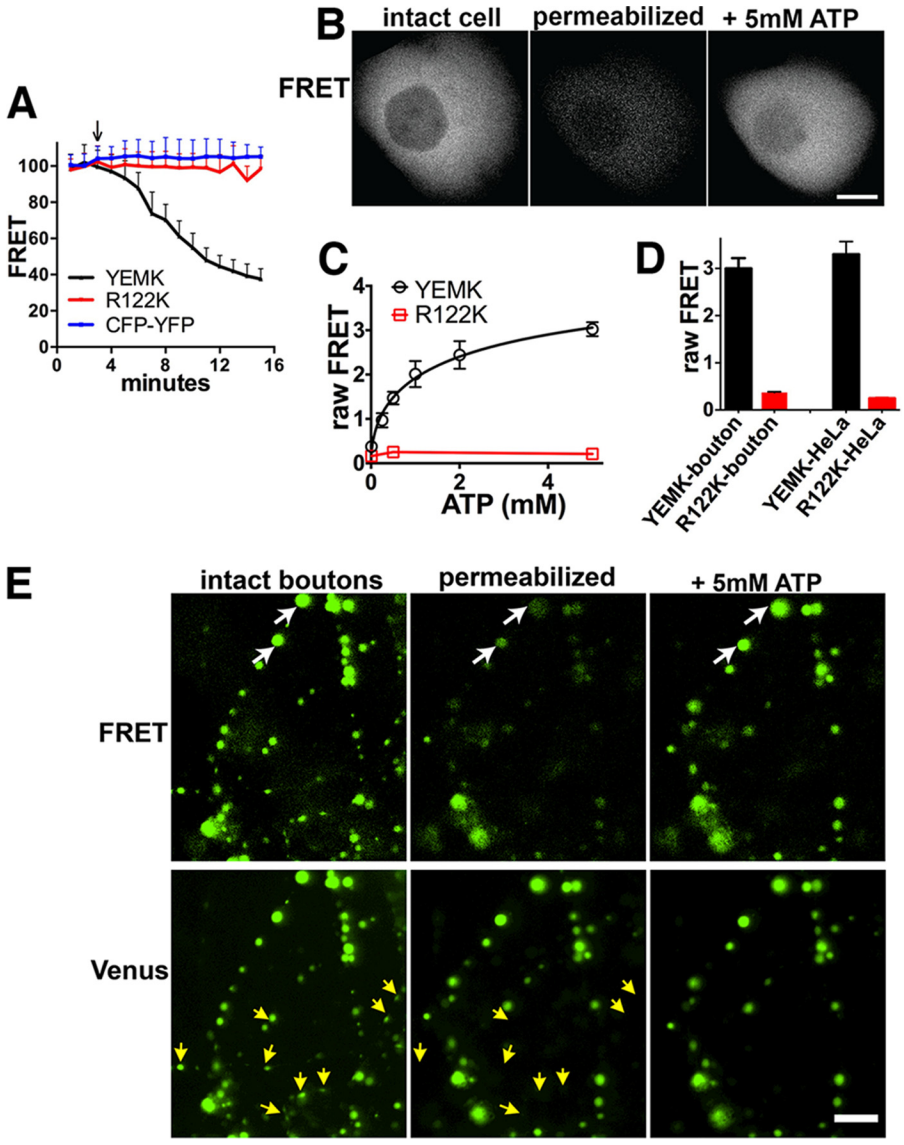

FIGURE 3. **Calibration of ATP sensors in cells.** *A,* FRET emission of HeLa cells expressing AT1.03^{YEMK} (ATP FRET sensor, YEMK, *black line*), AT$^{R122K/R126K}$ (R122K, a FRET sensor unresponsive to ATP (10), *red line*), or a direct CFP-YFP fusion control (*blue line*). Simultaneously inhibiting glycolysis with 2DG (10 mM) and oxidative phosphorylation with KCN (1 mM), indicated by the *arrow*, rapidly decreases relative ATP levels of ATP YEMK without affecting R122K. $n = 4–6$ coverslips/group, 3–6 cells/coverslip. Data are mean ± S.E. *B* and *C,* calibration of ATP FRET sensors in permeabilized cells. HeLa cells expressing AT1.03^{YEMK} or the AT$^{R122K/R126K}$ dead mutant were permeabilized with XF-PMP reagent (1 nM), and then ATP at defined concentrations was added. FRET was measured by microscopy, and the curve was fitted using a Hill equation. Data show mean ± S.D. *Scale bar,* 5 μm. *D,* comparison of raw FRET of ATP FRET sensor and dead mutant in intact HeLa cells and hippocampal boutons. *E,* hippocampal neuron boutons expressing the ATP FRET sensor were permeabilized by incubating in 1.25 nM XF-PMP reagent for 4 min and then bathed in 5 mM ATP. The FRET signal decreases markedly upon permeabilization and then returns upon exposure to ATP (*arrows*). However, during permeabilization, many boutons either detach or change shape/location (*yellow arrows*). In addition, the cytosolic buffer causes many boutons to swell rapidly, even before the permeabilization reagent is added. The fluorescence of the acceptor (Venus) protein in the ATP FRET sensor is unchanged. *Scale bar,* 5 μm.

pyruvate were present, but in pyruvate alone it produced a surprisingly greater drop in ATP with no recovery (Fig. 5, *A* and *B*), suggesting that this stimulation paradigm either failed to trigger compensatory synthesis of ATP (35) and/or impaired mitochondria's ability to synthesize ATP. Overall, these findings show that our ATP assay is sensitive enough to detect the energy requirements of physiologic stimuli, although we cannot exclude the possibility it would be even more sensitive if we could normalize for the total adenine nucleotide pool size (37). Indeed, ATP levels can be maintained by redistribution of the adenine nucleotide pool (38), although we know very little about the concentrations and kinetics of interconversion of adenine nucleotides within individual neurons and their subcellular compartments (39).

To confirm that the drop in FRET specifically reflected energy requirements of synaptic vesicle cycling and was not an artifact of electrical stimulation, we examined ATP levels in the absence of calcium (no-calcium buffer with EGTA). Here, electrical stimulation did not affect ATP levels (Fig. 5*C*), which corroborates recent data suggesting that synaptic vesicle cycling is the greatest user of ATP at the synapse (35).

The pHluorin experiments (Fig. 2) show that, unlike the final stages of exocytosis, endocytosis has a high ATP dependence. Because blocking mitochondrial ATP production caused

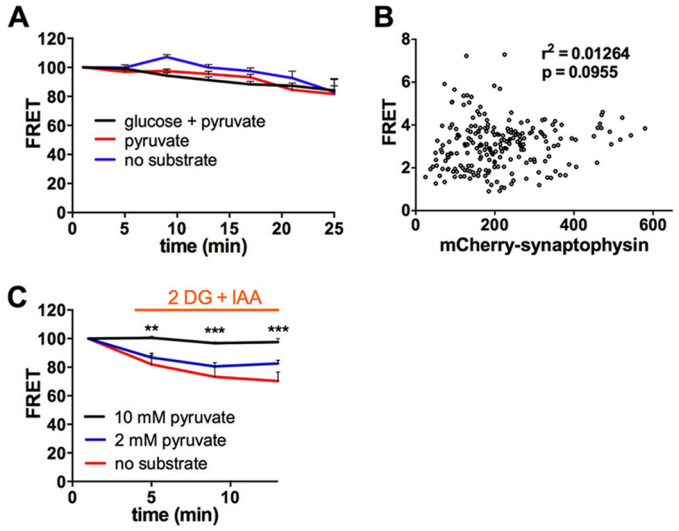

FIGURE 4. **Basal ATP levels at the nerve terminal can be supported by either glycolysis or aerobic respiration.** *A,* basal ATP was not affected by acute changes in substrate. ATP levels of hippocampal neuron boutons were assessed using ATP YEMK. At $t = 4$ min, media were changed from glucose (30 mM) and pyruvate (10 mM) to either pyruvate only (10 mM) or no substrate. Basal ATP levels remained similar in all groups, indicating that the remaining substrates are sufficient to maintain ATP at baseline in both compartments. $n = 6–8$ coverslips/group, with 15–20 boutons/coverslip. Data show mean ± S.E. *B,* ATP FRET measurements are independent of expression level. In synaptic boutons co-expressing ATP YEMK and mCherry-synaptophysin, linear regression was performed to assess the intensity of mCherry-synaptophysin (as a surrogate for extent of expression) and FRET. There was no significant correlation between the two variables. The square of the correlation coefficient (r^2) represents the proportion of variability in FRET that is accounted for by the initial YFP value. *C,* neurons require mitochondrially derived ATP when glycolysis is blocked. Basal ATP levels of synaptic boutons drop when glycolysis is blocked (using 2DG at 5 mM and IAA at 1 mM) and if pyruvate is absent. The decrease in ATP is prevented by 10 mM pyruvate but not 2 mM pyruvate. $n = 3–4$ coverslips/group, with 15–20 boutons/coverslip. Data are mean ± S.E. **, $p < 0.01$; ***, $p < 0.001$, *versus* no substrate group by two-way ANOVA and Tukey's post hoc test.

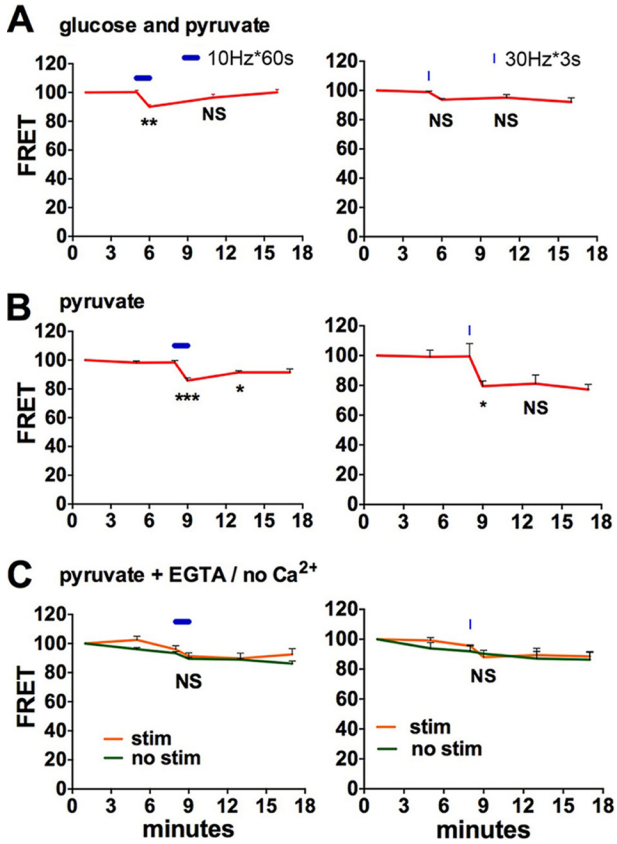

FIGURE 5. **Synaptic transmission decreases ATP at the synapse.** Hippocampal neurons expressing ATP FRET sensor and mCherry-synaptophysin (to identify synaptic boutons) were subjected to electrical field stimulation (*10Hz*60s*, *horizontal blue line* (*left column*); *30Hz*3s*, *narrow vertical blue line* (*right column*)). Individual synaptic boutons were imaged, and the FRET was calculated. *A,* when in both glucose (30 mM) and pyruvate (10 mM), electrical stimulation at 10Hz*60s produces a transient decrease in ATP that fully recovers ($n = 4$ coverslips/group), although 30Hz*3s has no detectable effect ($n = 5$ coverslips/group). *B,* in pyruvate alone, electrical stimulation with either paradigm produces a larger drop in ATP that shows partial (10Hz*60s group, $n = 8$ coverslips/group) or no (30Hz*3s group, $n = 7$ coverslips/group) recovery. 10–15 boutons/coverslip. Data show mean ± S.E. *NS* = not significant; *, $p < 0.05$; **, $p < 0.01$; ***, $p < 0.001$, not significant, *versus* time point immediately before stimulation by one-way ANOVA and Sidak's post hoc test. *C,* electrical stimulation in the absence of Ca^{2+} with 10 mM EGTA has no effect on ATP levels. *NS,* not significant, two-way ANOVA and Sidak's post hoc test.

pHluorin fluorescence to remain high after exocytosis (Fig. 2), energy depletion may have blocked endocytosis at or before vesicle scission or, in a subsequent step, prevented vesicles from becoming re-acidified. To distinguish between these possibilities, we first examined the ATP requirements of synaptic vesicle reacidification, a known energy-requiring process (40). However, bafilomycin (which blocks the reacidification of vesicles, Fig. 6*A*) did not affect the rate or extent of decrease in mitochondrially derived ATP produced by prolonged stimulation (10Hz*150s) (Fig. 6*B*), indicating that vesicle reacidification is not the primary ATP-consuming process.

To determine whether the block may instead occur proximal to reacidification at the vesicle reinternalization step, we next acutely added MES (pH 5.5) to see whether it quenched pHluorin fluorescence when endocytosis was blocked (Fig. 6*C*). We hypothesized that MES would not quench fluorescence if vesicles were blocked at the re-acidification stage because the vesicles would have already been internalized and therefore not accessible to MES. In contrast, MES would rapidly quench fluorescence if the block prevented vesicle scission. When we used rotenone to block endocytosis, MES rapidly quenched the increased pHluorin fluorescence, indicating that endocytosis requires high ATP at or before vesicle scission.

After establishing the stage at which synaptic vesicle cycling is blocked during energy failure, we used our ATP assay to define how much ATP is required for endocytosis (the ATP threshold). Defining this threshold would allow us to determine whether it is breached in models of neuronal dysfunction, which is critical for understanding whether energy failure truly impairs function and contributes to pathogenesis. We began defining this energy threshold by subjecting neurons to the same electrical stimulation patterns and non-glucose conditions that forced reliance on mitochondrially derived ATP in Fig. 2, *B* and *E*. Consistent with these results, the acute addition of rotenone decreased ATP levels faster in groups lacking glucose, especially with stimulation (Fig. 6, *D* and *E*), presumably because neurons could not adequately compensate with glycolysis. Therefore, after acutely blocking energy production, we found that the ATP threshold required to sustain endocytosis resides between the ATP level with and without glucose (Fig. 6, *D* and *E*). Based on our calibration in HeLa cells (Fig. 3), we estimate this ATP threshold to be ≈0.8 mM.

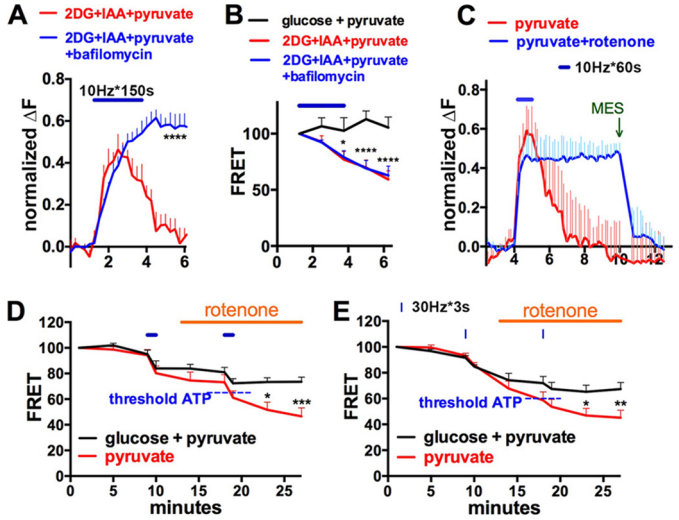

FIGURE 6. **Acute block of respiratory function decreases mitochondrially derived ATP below the threshold level for endocytosis.** *A,* acute treatment with bafilomycin (1 μM) inhibits the reacidification of synaptic vesicles after extended stimulation (10Hz*150s, *blue bar* in *A* and *B*), assessed with VGLUT1-pHluorin, and performed in pyruvate without glycolysis (2DG and IAA) to force reliance on mitochondrially derived ATP. $n = 6$ coverslips/group, with 10–16 boutons/coverslip. Data show mean ± S.E. ****, $p < 0.0001$ *versus* no bafilomycin control group by unpaired two-tailed *t* test for extent of endocytosis ((amplitude endocytosis)/(amplitude exocytosis)). *B,* inhibition of reacidification by bafilomycin does not prevent the decrease in ATP levels as compared with the no-bafilomycin control group, indicating that this step of vesicle cycling requires comparatively little energy. $n = 5–9$ coverslips/group, with 10–15 boutons/coverslip. Data show mean ± S.E. *, $p < 0.05$; ****, $p < 0.0001$ *versus* glucose + pyruvate by two-way ANOVA with repeated measures and Bonferroni post hoc test. *C,* pre-exposing neurons to rotenone before stimulation in pyruvate buffer (10 mM) blocked endocytosis, but MES (25 mM, pH 5.5), which acidifies the extracellular compartment, rapidly quenched fluorescence, indicating that endocytosis was blocked at or before the vesicle scission step. Electrical field stimulation alone (*D,* 10Hz*60s; *E,* 30Hz*3s) acutely decreased ATP similarly in the presence or absence of glucose (buffer switched to pyruvate without glucose at $t = 4$ min). When rotenone (*orange line*, beginning after the initial stimulation) was added to impair mitochondrial function, ATP decreased more in cultures without glucose, presumably because these cells could not compensate with glycolysis. $n = 9–11$ coverslips/group, with 15–20 boutons/coverslip. Data show mean ± S.E. *, $p < 0.05$; **, $p < 0.01$; ***, $p < 0.001$ *versus* glucose by two-way ANOVA with repeated measures and Bonferroni post hoc test.

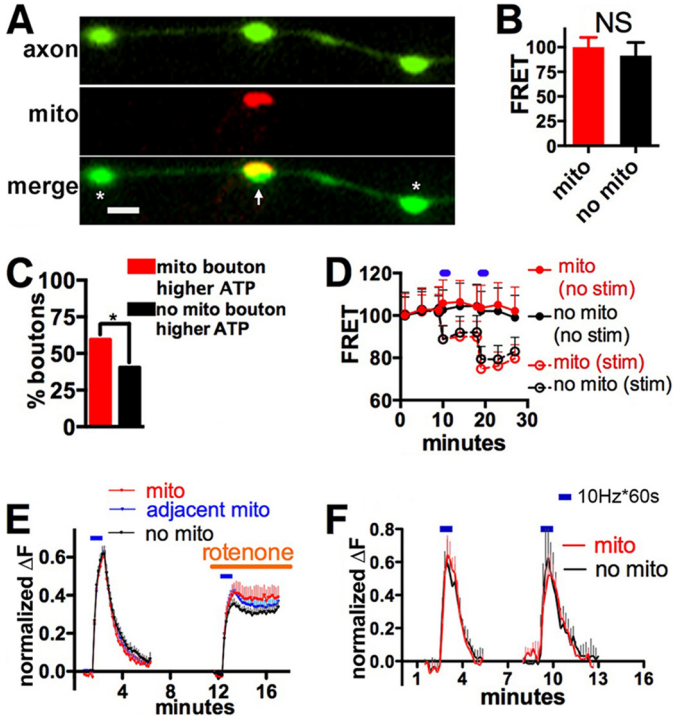

FIGURE 7. **Mitochondrially derived ATP diffuses from adjacent boutons to maintain synaptic function in boutons lacking mitochondria.** *A,* individual synaptic boutons labeled by ATP sensor (Venus channel), with and without mitochondria, identified by mito-FarRed fluorescence. The axon has a bouton containing a mitochondrion (*mito*) (*arrow*) next to two boutons without mitochondria (*). *Scale bar,* 2 μm. *B,* in total, ATP FRET levels did not differ significantly between boutons with and without mitochondria, despite being imaged in pyruvate (no glucose) to minimize glycolysis. *NS* ($p = 0.52$) by unpaired two-tailed *t* test. *C,* without glucose, ATP levels were also examined in adjacent boutons of sparsely transfected hippocampal cultures to unambiguously identify individual axons and their mitochondria. In ≈60% of cases, boutons with mitochondria had slightly higher ATP (*mito bouton higher ATP*) than adjacent boutons without mitochondria in the same axon $n = 15–16$ coverslips (15–20 boutons)/coverslip ($p < 0.05$ by binomial test). *D,* electrical field stimulation (*10Hz*60s*, *blue lines*) decreased ATP similarly in boutons with and without mitochondria. Data show mean ± S.E., $n = 15–16$ coverslips/group, 15–20 boutons/coverslip with and without mitochondria. *E,* VGLUT1-pHluorin fluorescence of neurons in pyruvate (10 mM; no glucose) subjected to electrical field stimulation (*10Hz*60s*, *blue line*). Boutons with mitochondria (+*mito*, identified by mito-mTagBFP), immediately adjacent to mitochondria (*adjacent mito*), and without mitochondria (*no mito*) respond similarly. $n = 6$ coverslips/group. *F,* synaptic transmission was examined in sparsely transfected hippocampal cultures to unambiguously identify individual axons and their mitochondria. Synaptic vesicle cycling was equivalent in boutons with and without mitochondria. $n = 6$ coverslips, 10–20 boutons/coverslip.

Diffusion Keeps Mitochondrion-derived ATP above the ATP Threshold for Synaptic Transmission, Even in Boutons Lacking Mitochondria—At the nerve terminal, energy failure may result from either intrinsic deficits in mitochondrial function or changes in the mass and/or distribution of mitochondria at the synapse. But even under normal conditions, only ≈39% of hippocampal boutons in our cultures contain mitochondria (109 boutons sampled from 10 coverslips), consistent with the ≈40% estimated by prior EM studies *in vivo* (2, 3). Thus, we asked whether ATP levels are lower in boutons without mitochondria. If so, do they meet the ATP threshold to perform synaptic vesicle cycling?

To test this, we first compared mitochondrially derived ATP levels in boutons with and without mitochondria, identified using mito-FarRed fluorescence, and imaged in pyruvate without glucose to force reliance on mitochondrially derived ATP (Fig. 7*A*). Notably, roughly 30% of axonal mitochondria are moving in our rat neuronal cultures (41). Therefore, to determine the impact of synaptic mitochondria on ATP, we only compared those boutons with or without stationary mitochondria. Specifically, boutons were considered to contain a stationary mitochondrion if the mitochondrion was present in the bouton at the beginning and end of the imaging period. Indeed, among these boutons, all of the mitochondria did indeed remain stationary in the bouton throughout the 33-min imaging period ($n = 25$, five boutons/coverslip based on a parallel experiment where mitochondria were imaged every 30 s). Boutons were considered not to have a mitochondrion if it was absent at the beginning and end of the imaging period, although those boutons that contained a mitochondrion only at the beginning or end of the imaging period were excluded from analysis. Using this approach, we found no significant difference in the ATP levels of the boutons (Fig. 7*B*). When we compared mitochondrially derived ATP levels within the same axon (a more sensitive approach), we found that ATP levels were

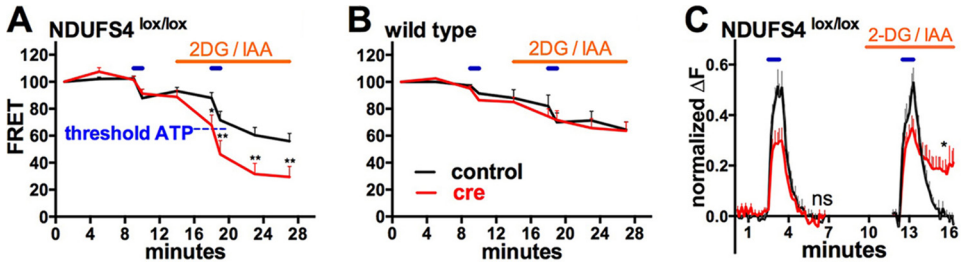

FIGURE 8. **Loss of a mitochondrial disease protein (NDUFS4, Leigh disease) causes energy failure at the synapse.** *A,* ATP levels in individual boutons of hippocampal neurons from floxed *Ndufs4* mice, with or without Cre (to delete *NDUFS4*). Neurons in pyruvate (no glucose) underwent electrical field stimulation (10Hz*60 s, *blue line*), first alone and then in the presence of 2DG (5 mM) and IAA (1 mM). After the initial stimulation, ATP dropped similarly in both groups. Once glycolysis was blocked, ATP dropped more in cells lacking *NDUFS4*, especially when we applied electrical activity (mimicking neural activity) to increase energy demands. $n = 12$ coverslips/group, with 15–20 boutons/coverslip. Data show mean ± S.E. **, $p < 0.01$ *versus* control. *B,* in neurons from wild-type mice, Cre expression did not affect ATP levels. $n = 10$–12 coverslips/group, with 15–20 boutons/coverslip. *C,* synaptic vesicle release in hippocampal neurons from floxed *Ndufs4* mice expressing VGLUT1-pHluorin. Neurons lacking *NDUFS4* had normal exocytosis but with a lower maximal amplitude. Inhibiting glycolysis with 2DG and IAA blocked endocytosis in neurons lacking *NDUFS4* but not control neurons, indicating that mitochondrially derived ATP could not maintain endocytosis when *NDUFS4* was deleted. $n = 9$–13 coverslips, 15–20 boutons/coverslip)/group. Data show mean ± S.E. *, $p < 0.05$ *versus* control. *ns* = not significant.

usually only slightly lower in adjacent boutons without mitochondria (Fig. 7*C*). Even after multiple stimulations to increase the energy requirements, ATP levels dropped similarly in boutons with and without mitochondria (Fig. 7*D*).

Thus, under normal conditions, ATP or ATP equivalents (42) diffuse rapidly into adjacent boutons to support synaptic function. These data suggest that boutons with and without mitochondria have similar amounts of mitochondrially derived ATP to support synaptic vesicle release. To confirm this, we compared synaptic vesicle cycling in boutons with and without mitochondria (again imaged in pyruvate without glucose to force reliance on mitochondrially derived ATP). As expected, synaptic vesicle cycling was identical in these boutons, and inhibiting respiration with rotenone blocked endocytosis similarly in boutons with and without mitochondria (Fig. 7*E*). Importantly, we identified mitochondria by their co-expression of mito-mTagBFP, and all mito-mTagBFP-positive structures tested (30 out of 30) were immunopositive for the mitochondrial marker Tom20. This approach ensured that we considered only mitochondria within transfected neurons, which was essential for definitively determining that mitochondria were present within a given axon (43). To prevent false-negatives (*i.e.* to make sure all mitochondrion-negative boutons truly lacked mitochondria), we optimized transfections so that the axons expressing VGLUT1-pHluorin also expressed our mitochondrial reporter (96% of pHluorin-positive axons also expressed mito-mTagBFP; $n = 49$ individual axons quantified). To further ensure that we accurately categorized boutons, we also examined sparsely transfected neurons. These experiments on single axons again showed that synaptic transmission was identical in boutons with and without mitochondria (Fig. 7*F*). Overall, we found that mitochondrially derived ATP levels in boutons without mitochondria exceed the ATP threshold required for synaptic vesicle cycling, and the small difference in mitochondrially derived ATP between these boutons has little functional consequence under the conditions tested. Thus, boutons without mitochondria have a similar capacity for synaptic vesicle cycling as those with mitochondria. Also, when energy requirements can not be met, energy failure occurs similarly in boutons with and without mitochondria, at least when the boutons are normally distributed.

Chronic Impairment in Mitochondrial Function Can Produce Energy Failure in Individual Neurons—In neurodegenerative diseases, mitochondrial function is chronically impaired, and hence, the requirement for mitochondrially derived ATP for synaptic transmission may differ from that after an acute respiratory insult. However, despite being a central hypothesis in neurodegeneration (6), no study has proved that ATP decreases in individual neurons in any model of neurodegeneration. We do not know whether and when this ATP drop occurs, or whether it is enough to compromise function. To determine how a chronic deficit in mitochondrial function affects mitochondrially derived ATP, we cultured hippocampal neurons from floxed *Ndufs4* mice (19). The *NDUFS4* protein, NADH dehydrogenase (ubiquinone) iron-sulfur protein 4, is an essential subunit of mitochondrial complex I. Deleting this gene produces devastating neurologic consequences in humans (44) and mice (19, 45) and severely impairs respiration in mesencephalic neurons (46). However, cultured dopaminergic neurons that lack *NDUFS4* due to Cre-mediated gene inactivation have normal survival (46, 47). Therefore, in standard culture conditions, even a severe mitochondrial deficit may be obscured, suggesting that standard culture paradigms are insensitive to the toxicity of mitochondrion-based energy failure. To test this, we co-transfected floxed *Ndufs4* hippocampal neurons with Cre (to delete *NDUFS4*), mCherry-synaptophysin, and either the ATP FRET sensor or VGLUT1-pHluorin. We previously optimized our transfection conditions so >90% of axons that express these reporter probes also express Cre.

In standard high glucose conditions, deleting *NDUFS4* in hippocampal neurons did not affect basal synaptic ATP FRET levels (controls, 2.74 ± 0.79; *NDUFS4*-depleted cells, 3.14 ± 0.34), suggesting that the neurons compensated with glycolysis. Surprisingly, in the acute absence of glucose, there was also no difference in response to an initial 10Hz*60s stimulation (Fig. 8*A*), suggesting that neurons with chronic respiratory defects may up-regulate their glycolytic capacity and/or endogenous glucose stores. However, after we added glycolytic inhibitors (2DG and iodoacetic acid (IAA)) to fully block glycolysis, ATP levels in *NDUFS4*-depleted boutons dropped more rapidly in response to a second electrical stimulation (Fig. 8*A*). Cre expression alone did not affect ATP levels in control neurons

(Fig. 8*B*), confirming that *NDUFS4* loss is responsible for the drop in ATP. To determine whether mitochondrially derived ATP drops enough in *NDUFS4*-depleted neurons to impair endocytosis, we examined synaptic vesicle cycling in floxed *Ndufs4* mice. Indeed, *NDUFS4*-depleted boutons had impaired endocytosis (Fig. 8*C*), mimicking the effects of acute complex I inhibition on control neurons in the absence of glucose (Fig. 2). Therefore, mitochondrially derived ATP levels are indeed compromised when *NDUFS4* is deleted, and they drop enough to impair synaptic transmission. This establishes that mitochondrion-based energy failure can occur in individual neurons in a genetic model of neurodegeneration.

Discussion

To determine whether changes in mitochondrial bioenergetics contribute to neurodegeneration (6), we must first understand the normal energy requirements for neuronal function and survival and determine whether and how energy levels change when mitochondria are compromised. Using new assays that provide complementary measures of mitochondrially derived ATP at the nerve terminal, a region that is compromised early in neurodegeneration (4, 5), we define the energy thresholds needed to sustain different phases of the synaptic vesicle cycle, and we show that under normal conditions enough mitochondrially derived ATP disperses rapidly between boutons to support synaptic function, even in boutons that lack mitochondria. But we also show that acutely or chronically inhibiting the respiratory chain drops mitochondrially derived ATP levels below the threshold needed to sustain endocytosis, especially when energy consumption is increased by greater neural activity. Thus, a chronic mitochondrial deficit that arises from losing a key mitochondrial protein, NDUFS4, which is lost in the neurodegenerative disorder Leigh disease (44), can indeed cause energy failure in individual neurons.

Normal Requirement and Dispersal of ATP at the Nerve Terminal—In neurons, most ATP is likely dedicated to supporting synaptic transmission. However, the energy requirements of the synaptic vesicle cycle are poorly understood. Our studies show that endocytosis is far more sensitive to mitochondrial ATP levels than exocytosis. Furthermore, we found that re-acidification is not the key energy-requiring step, consistent with recent theoretical estimates of the ATP requirements of synaptic vesicle reacidification (48). Instead, the vesicle scission phase of endocytosis has high energy requirements, consistent with studies that showed ATP is required for the scission of coated pits into sealed vesicles in mammalian cell lines (49) and for membrane fission and/or retrieval in goldfish bipolar neurons (50). Indeed, attenuating endocytosis may help neurons preserve ATP when needed, as synaptic vesicle cycling likely uses much of the ATP at the synapse (Fig. 5 (35)). Further studies will be required to determine specifically how low ATP limits vesicle scission. In contrast to endocytosis, we show that vesicle release from the readily releasable pool requires little ATP, which is consistent with studies in permeabilized endocrine cells and goldfish retinal bipolar neurons, showing that once "primed," vesicle release is independent of ATP but depends on Ca^{2+} (51). Although endocytosis is far more sensitive to decreased energy than exocytosis, some ATP is still needed to facilitate exocytosis, presumably in part due to the ATPase activity of the *N*-ethylmaleimide-sensitive factor (NSF), which is required before vesicle fusion (52).

To sustain the synaptic vesicle cycle, ATP must first reach the nerve terminals, which are often located far from the cell body. Although the cell body's mitochondria may produce some ATP that diffuses to the nerve terminal as phosphocreatine (42), long distance energy transport probably does not contribute much energy at the synapse; in fact, it would make neurons unable to rapidly adjust their energy production to meet local needs. Instead, regional mitochondria in axons probably supply most of the energy at the synapse (53). Indeed, we show that when mitochondria are normally distributed and functioning, enough mitochondrially derived ATP can diffuse to maintain normal function even in boutons that lack mitochondria. This does not preclude the possibility that regional gradients of glycolytically derived ATP exist within axons to fuel specialized functions such as axonal transport (54), but such gradients are beyond the detection limit of our assay. These findings thus offer some of the first insights into how boutons that lack mitochondria function. Also, we show that when energy requirements are increased sufficiently, energy failure occurs to a similar extent in boutons with and without mitochondria, even under conditions where the boutons are forced to rely on their mitochondria for ATP. Nonetheless, more sustained increases in energy demands may still preferentially deplete ATP from boutons lacking mitochondria. Indeed, after multiple rounds of electrical stimulation, Sun *et al.* (55) found that the ATP/ADP ratio decreased more in boutons lacking mitochondria, despite having glucose present. In addition, we do not yet know whether regional energy failure between boutons also develops if the distance between mitochondria is pathologically increased (6).

Energy Failure at the Synapse in Neurodegeneration—Defects in mitochondrial bioenergetics likely influence the pathogenesis of many neurodegenerative diseases, including Parkinson disease, Huntington disease, and Alzheimer disease (6). Energy status at the synapse may be particularly important because in most neurons most mitochondria likely reside in axons (56), and degeneration begins in this compartment (4, 5). Even before synapses are lost, insufficient ATP may contribute to early disease-related changes in synaptic transmission (27, 57). However, energy failure has never been directly proven in affected neurons in these diseases or even in intact neurons in genetic models of these diseases, leaving the central tenet of the bioenergetic hypothesis unproven (6, 22).

The recent emergence of fluorescent sensors for energy metabolites allows us to interrogate energy status on a single-cell basis (10, 58); here, we show that this technology can be applied to individual living neurons and their synapses. Our results show that chronic, genetic loss of mitochondrial function can lead to energy failure, although energy failure will only occur when glycolysis is limited and neurons are forced to rely more heavily on their mitochondria, as likely occurs *in vivo* (6). In the brain, glucose levels are far lower than in standard neuronal culture (25, 26), and neurons *in vivo* likely derive a greater proportion of their energy from aerobic respiration. Much of this ATP may be generated from lactate produced by adjacent

glial cells and then imported into neurons via the astrocyte-neuron lactate shuttle, where it is converted into pyruvate (28, 59). However, recent evidence suggests that neurons (not astrocytes) directly metabolize much of the glucose entering the brain (60, 61), suggesting that glycolysis may actually contribute more to supporting neuronal energy needs than previously suspected. Importantly, we must better understand the role of energy failure in neurodegeneration because mitochondria have other functions; they buffer calcium, produce reactive oxygen species, synthesize lipids, and regulate apoptosis (62). How these other functions affect synapses is even less well understood than bioenergetics. If a given disease mutation does not violate a neuron's energy threshold, then energy failure is probably not the main way the mutation produces degeneration. Conversely, if energy levels dip below the threshold, insufficient energy may help cause degeneration (6). As such, our assays may eventually be used to test therapeutic interventions that restore energy levels.

Author Contributions—D. P., L. S., B. A. M., A. A. G., M. D. B., R. H.E., and K. N. designed research. D. P., L. S., B. A. M., D. H., W. L., A. A. G., and K. N. performed research. D. P., L. S., B. A. M., D. H., A. A. G., H. K., and K. N. analyzed data. D. P., L. S., B. A. M., A. A. G., and K. N. wrote the paper.

Acknowledgments—We thank Richard Palmiter (University of Washington, Seattle) for the floxed Ndufs4 mice and for critically reviewing our manuscript. We thank Gary Howard and Celeste Brennecka for helping edit the manuscript, and the S. D. Bechtel Junior Foundation for their gift of a Seahorse Analyzer to the Gladstone Institutes.

References

1. Harris, J. J., Jolivet, R., and Attwell, D. (2012) Synaptic energy use and supply. *Neuron* **75,** 762–777
2. Shepherd, G. M., and Harris, K. M. (1998) Three-dimensional structure and composition of CA3→CA1 axons in rat hippocampal slices: implications for presynaptic connectivity and compartmentalization. *J. Neurosci.* **18,** 8300–8310
3. Kang, J. S., Tian, J. H., Pan, P. Y., Zald, P., Li, C., Deng, C., and Sheng, Z. H. (2008) Docking of axonal mitochondria by syntaphilin controls their mobility and affects short-term facilitation. *Cell* **132,** 137–148
4. Scheff, S. W., Price, D. A., Schmitt, F. A., DeKosky, S. T., and Mufson, E. J. (2007) Synaptic alterations in CA1 in mild Alzheimer disease and mild cognitive impairment. *Neurology* **68,** 1501–1508
5. Cheng, H. C., Ulane, C. M., and Burke, R. E. (2010) Clinical progression in Parkinson disease and the neurobiology of axons. *Ann. Neurol.* **67,** 715–725
6. Pathak, D., Berthet, A., and Nakamura, K. (2013) Energy failure: does it contribute to neurodegeneration? *Ann. Neurol.* **74,** 506–516
7. Choi, S. W., Gerencser, A. A., Lee, D. W., Rajagopalan, S., Nicholls, D. G., Andersen, J. K., and Brand, M. D. (2011) Intrinsic bioenergetic properties and stress sensitivity of dopaminergic synaptosomes. *J. Neurosci.* **31,** 4524–4534
8. Verburg, J., and Hollenbeck, P. J. (2008) Mitochondrial membrane potential in axons increases with local nerve growth factor or semaphorin signaling. *J. Neurosci.* **28,** 8306–8315
9. Voglmaier, S. M., Kam, K., Yang, H., Fortin, D. L., Hua, Z., Nicoll, R. A., and Edwards, R. H. (2006) Distinct endocytic pathways control the rate and extent of synaptic vesicle protein recycling. *Neuron* **51,** 71–84
10. Imamura, H., Nhat, K. P., Togawa, H., Saito, K., Iino, R., Kato-Yamada, Y., Nagai, T., and Noji, H. (2009) Visualization of ATP levels inside single living cells with fluorescence resonance energy transfer-based genetically encoded indicators. *Proc. Natl. Acad. Sci. U.S.A.* **106,** 15651–15656
11. Hua, Z., Leal-Ortiz, S., Foss, S. M., Waites, C. L., Garner, C. C., Voglmaier, S. M., and Edwards, R. H. (2011) v-SNARE composition distinguishes synaptic vesicle pools. *Neuron* **71,** 474–487
12. Nakamura, K., Nemani, V. M., Wallender, E. K., Kaehlcke, K., Ott, M., and Edwards, R. H. (2008) Optical reporters for the conformation of α-synuclein reveal a specific interaction with mitochondria. *J. Neurosci.* **28,** 12305–12317
13. Nakamura, K., Nemani, V. M., Azarbal, F., Skibinski, G., Levy, J. M., Egami, K., Munishkina, L., Zhang, J., Gardner, B., Wakabayashi, J., Sesaki, H., Cheng, Y., Finkbeiner, S., Nussbaum, R. L., Masliah, E., and Edwards, R. H. (2011) Direct membrane association drives mitochondrial fission by the Parkinson disease-associated protein α-synuclein. *J. Biol. Chem.* **286,** 20710–20726
14. Morozova, K. S., Piatkevich, K. D., Gould, T. J., Zhang, J., Bewersdorf, J., and Verkhusha, V. V. (2010) Far-red fluorescent protein excitable with red lasers for flow cytometry and superresolution STED nanoscopy. *Biophys. J.* **99,** L13–L15
15. Subach, O. M., Gundorov, I. S., Yoshimura, M., Subach, F. V., Zhang, J., Grüenwald, D., Souslova, E. A., Chudakov, D. M., and Verkhusha, V. V. (2008) Conversion of red fluorescent protein into a bright blue probe. *Chem. Biol.* **15,** 1116–1124
16. Nemani, V. M., Lu, W., Berge, V., Nakamura, K., Onoa, B., Lee, M. K., Chaudhry, F. A., Nicoll, R. A., and Edwards, R. H. (2010) Increased expression of α-synuclein reduces neurotransmitter release by inhibiting synaptic vesicle reclustering after endocytosis. *Neuron* **65,** 66–79
17. Onoa, B., Li, H., Gagnon-Bartsch, J. A., Elias, L. A., and Edwards, R. H. (2010) Vesicular monoamine and glutamate transporters select distinct synaptic vesicle recycling pathways. *J. Neurosci.* **30,** 7917–7927
18. Berthet, A., Margolis, E. B., Zhang, J., Hsieh, I., Zhang, J., Hnasko, T. S., Ahmad, J., Edwards, R. H., Sesaki, H., Huang, E. J., and Nakamura, K. (2014) Loss of mitochondrial fission depletes axonal mitochondria in midbrain dopamine neurons. *J. Neurosci.* **34,** 14304–14317
19. Kruse, S. E., Watt, W. C., Marcinek, D. J., Kapur, R. P., Schenkman, K. A., and Palmiter, R. D. (2008) Mice with mitochondrial complex I deficiency develop a fatal encephalomyopathy. *Cell Metab.* **7,** 312–320
20. Deleted in proof
21. Yao, J., Chen, S., Mao, Z., Cadenas, E., and Brinton, R. D. (2011) 2-Deoxy-D-glucose treatment induces ketogenesis, sustains mitochondrial function, and reduces pathology in female mouse model of Alzheimer's disease. *PLoS ONE* **6,** e21788
22. Choi, S. W., Gerencser, A. A., Ng, R., Flynn, J. M., Melov, S., Danielson, S. R., Gibson, B. W., Nicholls, D. G., Bredesen, D. E., and Brand, M. D. (2012) No consistent bioenergetic defects in presynaptic nerve terminals isolated from mouse models of Alzheimer's disease. *J. Neurosci.* **32,** 16775–16784
23. Tanaka, T., Nagashima, K., Inagaki, N., Kioka, H., Takashima, S., Fukuoka, H., Noji, H., Kakizuka, A., and Imamura, H. (2014) Glucose-stimulated single pancreatic islets sustain increased cytosolic ATP levels during initial Ca^{2+} influx and subsequent Ca2+ oscillations. *J. Biol. Chem.* **289,** 2205–2216
24. Xia, Z., and Liu, Y. (2001) Reliable and global measurement of fluorescence resonance energy transfer using fluorescence microscopes. *Biophys. J.* **81,** 2395–2402
25. McNay, E. C., Fries, T. M., and Gold, P. E. (2000) Decreases in rat extracellular hippocampal glucose concentration associated with cognitive demand during a spatial task. *Proc. Natl. Acad. Sci. U.S.A.* **97,** 2881–2885
26. Rex, A., Bert, B., Fink, H., and Voigt, J. P. (2009) Stimulus-dependent changes of extracellular glucose in the rat hippocampus determined by *in vivo* microdialysis. *Physiol. Behav.* **98,** 467–473
27. Yasuda, T., Nakata, Y., Choong, C. J., and Mochizuki, H. (2013) Neurodegenerative changes initiated by presynaptic dysfunction. *Transl. Neurodegener.* **2,** 16
28. Pellerin, L., and Magistretti, P. J. (2012) Sweet sixteen for ANLS. *J. Cereb. Blood Flow Metab.* **32,** 1152–1166
29. Mozhayeva, M. G., Sara, Y., Liu, X., and Kavalali, E. T. (2002) Development of vesicle pools during maturation of hippocampal synapses. *J. Neurosci.* **22,** 654–665

30. Sudhof, T. C., and Rizo, J. (2011) Synaptic vesicle exocytosis. *Cold Spring Harb. Perspect. Biol.* **3,** *10.1101/cshperspect.a005637*
31. Pyle, J. L., Kavalali, E. T., Piedras-Rentería, E. S., and Tsien, R. W. (2000) Rapid reuse of readily releasable pool vesicles at hippocampal synapses. *Neuron* **28,** 221–231
32. Vilchez, D., Ros, S., Cifuentes, D., Pujadas, L., Vallès, J., García-Fojeda, B., Criado-García, O., Fernández-Sánchez, E., Medraño-Fernández, I., Domínguez, J., García-Rocha, M., Soriano, E., Rodríguez de Córdoba, S., and Guinovart, J. J. (2007) Mechanism suppressing glycogen synthesis in neurons and its demise in progressive myoclonus epilepsy. *Nat. Neurosci.* **10,** 1407–1413
33. Imamura, H., and Noji, H. (2009) Imaging of intracellular ATP using novel fluorescent probes. *Tanpakushitsu Kakusan Koso* **54,** 1937–1944
34. Tsuyama, T., Kishikawa, J., Han, Y. W., Harada, Y., Tsubouchi, A., Noji, H., Kakizuka, A., Yokoyama, K., Uemura, T., and Imamura, H. (2013) *In vivo* fluorescent adenosine 5′-triphosphate (ATP) imaging of *Drosophila melanogaster* and *Caenorhabditis elegans* by using a genetically encoded fluorescent ATP biosensor optimized for low temperatures. *Anal. Chem.* **85,** 7889–7896
35. Rangaraju, V., Calloway, N., and Ryan, T. A. (2014) Activity-driven local ATP synthesis is required for synaptic function. *Cell* **156,** 825–835
36. Lin, R. Y., Vera, J. C., Chaganti, R. S., and Golde, D. W. (1998) Human monocarboxylate transporter 2 (MCT2) is a high affinity pyruvate transporter. *J. Biol. Chem.* **273,** 28959–28965
37. Ball, W. J., Jr., and Atkinson, D. E. (1975) Adenylate energy charge in *Saccharomyces cerevisiae* during starvation. *J. Bacteriol.* **121,** 975–982
38. Brand, M. D., and Nicholls, D. G. (2011) Assessing mitochondrial dysfunction in cells. *Biochem. J.* **435,** 297–312
39. Erecińska, M., and Silver, I. A. (1989) ATP and brain function. *J. Cereb. Blood Flow Metab.* **9,** 2–19
40. Budzinski, K. L., Zeigler, M., Fujimoto, B. S., Bajjalieh, S. M., and Chiu, D. T. (2011) Measurements of the acidification kinetics of single SynaptopHluorin vesicles. *Biophys. J.* **101,** 1580–1589
41. Hertz, N. T., Berthet, A., Sos, M. L., Thorn, K. S., Burlingame, A. L., Nakamura, K., and Shokat, K. M. (2013) A neo-substrate that amplifies catalytic activity of Parkinson's-disease-related kinase PINK1. *Cell* **154,** 737–747
42. Kuiper, J. W., Oerlemans, F. T., Fransen, J. A., and Wieringa, B. (2008) Creatine kinase B deficient neurons exhibit an increased fraction of motile mitochondria. *BMC Neurosci.* **9,** 73
43. Waters, J., and Smith, S. J. (2003) Mitochondria and release at hippocampal synapses. *Pflugers Arch.* **447,** 363–370
44. Leshinsky-Silver, E., Lebre, A. S., Minai, L., Saada, A., Steffann, J., Cohen, S., Rötig, A., Munnich, A., Lev, D., and Lerman-Sagie, T. (2009) NDUFS4 mutations cause Leigh syndrome with predominant brainstem involvement. *Mol. Genet. Metab.* **97,** 185–189
45. Quintana, A., Zanella, S., Koch, H., Kruse, S. E., Lee, D., Ramirez, J. M., and Palmiter, R. D. (2012) Fatal breathing dysfunction in a mouse model of Leigh syndrome. *J. Clin. Invest.* **122,** 2359–2368
46. Choi, W. S., Kruse, S. E., Palmiter, R. D., and Xia, Z. (2008) Mitochondrial complex I inhibition is not required for dopaminergic neuron death induced by rotenone, MPP^+, or paraquat. *Proc. Natl. Acad. Sci. U.S.A.* **105,** 15136–15141
47. Choi, W. S., Palmiter, R. D., and Xia, Z. (2011) Loss of mitochondrial complex I activity potentiates dopamine neuron death induced by microtubule dysfunction in a Parkinson's disease model. *J. Cell Biol.* **192,** 873–882
48. Egashira, Y., Takase, M., and Takamori, S. (2015) Monitoring of vacuolar-type H^+ ATPase-mediated proton influx into synaptic vesicles. *J. Neurosci.* **35,** 3701–3710
49. Smythe, E., Pypaert, M., Lucocq, J., and Warren, G. (1989) Formation of coated vesicles from coated pits in broken A431 cells. *J. Cell Biol.* **108,** 843–853
50. Heidelberger, R. (2001) ATP is required at an early step in compensatory endocytosis in synaptic terminals. *J. Neurosci.* **21,** 6467–6474
51. Holz, R. W., Bittner, M. A., Peppers, S. C., Senter, R. A., and Eberhard, D. A. (1989) MgATP-independent and MgATP-dependent exocytosis. Evidence that MgATP primes adrenal chromaffin cells to undergo exocytosis. *J. Biol. Chem.* **264,** 5412–5419
52. Kuner, T., Li, Y., Gee, K. R., Bonewald, L. F., and Augustine, G. J. (2008) Photolysis of a caged peptide reveals rapid action of *N*-ethylmaleimide-sensitive factor before neurotransmitter release. *Proc. Natl. Acad. Sci. U.S.A.* **105,** 347–352
53. Verstreken, P., Ly, C. V., Venken, K. J., Koh, T. W., Zhou, Y., and Bellen, H. J. (2005) Synaptic mitochondria are critical for mobilization of reserve pool vesicles at *Drosophila* neuromuscular junctions. *Neuron* **47,** 365–378
54. Zala, D., Hinckelmann, M. V., Yu, H., Lyra da Cunha, M. M., Liot, G., Cordelières, F. P., Marco, S., and Saudou, F. (2013) Vesicular glycolysis provides on-board energy for fast axonal transport. *Cell* **152,** 479–491
55. Sun, T., Qiao, H., Pan, P. Y., Chen, Y., and Sheng, Z. H. (2013) Motile axonal mitochondria contribute to the variability of presynaptic strength. *Cell Rep.* **4,** 413–419
56. Grafstein, B., and Forman, D. S. (1980) Intracellular transport in neurons. *Physiol. Rev.* **60,** 1167–1283
57. Keating, D. J. (2008) Mitochondrial dysfunction, oxidative stress, regulation of exocytosis and their relevance to neurodegenerative diseases. *J. Neurochem.* **104,** 298–305
58. Berg, J., Hung, Y. P., and Yellen, G. (2009) A genetically encoded fluorescent reporter of ATP:ADP ratio. *Nat. Methods* **6,** 161–166
59. Nagase, M., Takahashi, Y., Watabe, A. M., Kubo, Y., and Kato, F. (2014) On-site energy supply at synapses through monocarboxylate transporters maintains excitatory synaptic transmission. *J. Neurosci.* **34,** 2605–2617
60. Patel, A. B., Lai, J. C., Chowdhury, G. M., Hyder, F., Rothman, D. L., Shulman, R. G., and Behar, K. L. (2014) Direct evidence for activity-dependent glucose phosphorylation in neurons with implications for the astrocyte-to-neuron lactate shuttle. *Proc. Natl. Acad. Sci. U.S.A.* **111,** 5385–5390
61. Lundgaard, I., Li, B., Xie, L., Kang, H., Sanggaard, S., Haswell, J. D., Sun, W., Goldman, S., Blekot, S., Nielsen, M., Takano, T., Deane, R., and Nedergaard, M. (2015) Direct neuronal glucose uptake heralds activity-dependent increases in cerebral metabolism. *Nat. Commun.* **6,** 6807
62. Nunnari, J., and Suomalainen, A. (2012) Mitochondria: in sickness and in health. *Cell* **148,** 1145–1159
63. Foss, S. M., Li, H., Santos, M. S., Edwards, R. H., and Voglmaier, S. M. (2013) Multiple dileucine-like motifs direct VGLUT1 trafficking. *J. Neurosci.* **33,** 10647–10660